Restrained vs Free Dynamics Simulations of Oligosaccharides: Application to Solution Dynamics of Biantennary and Bisected Biantennary N-Linked Glycans†

T. J. Rutherford and S. W. Homans*

Department of Biochemistry, University of Dundee, Dundee, DD1 4HN U.K.

Received March 29, 1994; Revised Manuscript Received May 12, 1994®

ABSTRACT: We have examined the dynamic behavior in solution of the biantennary glycan GlcNAcβ1-2Manα1-6(GlcNAcβ1-2Manα1-3)Manβ1-4GlcNAcβ1-4GlcNAc, and its "bisected" analogue GlcNAcβ1-2Manα1-6(GlcNAcβ1-2Manα1-3)(GlcNAcβ1-4)Manβ1-4GlcNAcβ1-4GlcNAc, by use of both free dynamics simulations and restrained dynamics simulations using distance restraints derived from ^{1}H NMR rotating frame Overhauser effect measurements. Data resulting from each type of simulation are compared with experimental data and are critically evaluated. Both methods suggest that most glycosidic linkages exhibit significant torsional oscillations in solution, and the dynamic behavior of certain linkages, notably Manα1–6Man and Manα1-3Man, were found to be restricted by the presence of the bisecting GlcNAc residue. The average structures so obtained were found to agree closely with those predicted in previous investigations where torsional oscillations about glycosidic linkages were not considered. In particular, the characteristic chemical shift perturbations induced by the bisecting GlcNAc residue could be explained in terms of the dynamic differences between the two glycans.

Early studies on the solution behavior of oligosaccharides led to the conclusion that the majority of glycosidic linkages in these moieties were essentially fixed in a single conformation (Lemieux et al., 1980; Bock et al., 1982; Homans et al., 1982; Thogersen et al., 1982; Bock, 1983; Brisson & Carver, 1983a–c; Homans et al., 1983; Sabesan et al., 1984; Paulsen et al., 1986; Homans et al., 1986; Homans et al., 1987a,b). However, more recent data have provided unequivocal evidence that this conclusion is not correct and that significant torsional oscillations exist about glycosidic linkages (Cumming & Carver, 1987a,b; Imberty et al., 1989; Homans, 1990; Yan & Bush, 1990; Bush & Cagas, 1992; Cagas & Bush, 1992; Bush, 1992; Miller et al., 1992, Poppe & van Halbeek, 1992; Imberty et al., 1993; Rutherford et al., 1993). In light of these data, it is therefore necessary to question the significance of all previous studies on the solution conformations of oligosaccharides where rigid geometry was assumed. In particular, it is necessary to evaluate the concept of "conformational transitions" (Homans et al., 1986), i.e., where the addition or deletion of one or more monosaccharide residues from a given glycan results in a significant conformational change either proximal or distal to the site of glycosylation. Whereas such transitions were previously interpreted in terms of discrete, fixed conformations, the question now arises as to how these changes, and the modifications in chemical shift, nuclear Overhauser effects, and spin–spin couplings to which they give rise in proton NMR spectra, can be interpreted in terms of a motional model.

A fundamental difficulty in addressing this question concerns the accuracy with which it is possible to define oligosaccharide solution dynamics, either theoretically or experimentally. Free molecular dynamics simulations have been extensively used to probe the extent of internal motions in oligosaccharides and their time scale, and their validity has in some studies been addressed by the back-calculation of NMR parameters (NOEs and coupling constants) from them for comparison with experiment (Homans & Forster, 1992; Rutherford et al., 1993). To our knowledge no such calculations have to date yielded back-calculated parameters which are in good agreement with experiment. A possible explanation for this poor performance is that currently accessible simulation times are of insufficient length to explore φ, ψ conformational space fully and thus reproduce adequately the relevant NMR parameters. However, it is also necessary to question the performance of current molecular mechanical force field parametrizations for oligosaccharides over the complete potential surface. That current parametrizations are inadequate is exemplified by the fact that back-calculated NMR data derived from statistical–mechanical analysis of gridsearch calculations, where the φ, ψ potential surface is by definition fully explored to a good approximation, do not correspond with experimental values even for simple disaccharides (Imberty et al., 1991).

Recently, we applied molecular dynamics simulations including weak distance restraints in a study of the solution dynamics of a model disaccharide (Rutherford et al., 1993). We found that such simulations were able to reproduce to reasonable accuracy not only the experimental magnitudes of the NOE restraints, but also long-range ^{13}C–^{1}H interresidue spin-coupling constants, despite the absence of angular restraints during the simulation. Although there are inherent caveats in this approach, which we further discuss in detail below, these data suggested that the restrained dynamics simulations might yield a good approximation to the true dynamic behavior of the molecule. In order to examine this concept further, here we examine the dynamic behavior of two biosynthetically related N-linked glycans, namely the biantennary glycan GlcNAcβ1-2Manα1-6(GlcNAcβ1-2Manα1-3)Manβ1-4GlcNAcβ1-4GlcNAc and its bisected couterpart GlcNAcβ1-2Manα1-6(GlcNAcβ1-2Manα1-3)(GlcNAcβ1-4)Manβ1-4GlcNAcβ1-4GlcNAc, using both free and restrained molecular dynamics techniques, followed by back-calculation of NMR data to examine the validity of each. These glycans have been chosen since the bisecting GlcNAc

† This work was funded by the LINK Biotransformations program of the Science and Engineering Research Council and The Department of Trade and Industry and by Celltech, Glaxo, ICI, and The Wellcome Foundation. S.W.H. is a Lister Institute Centenary Research Fellow.

® Abstract published in *Advance ACS Abstracts,* July 15, 1994.

0006-2960/94/0433-9606$04.50/0

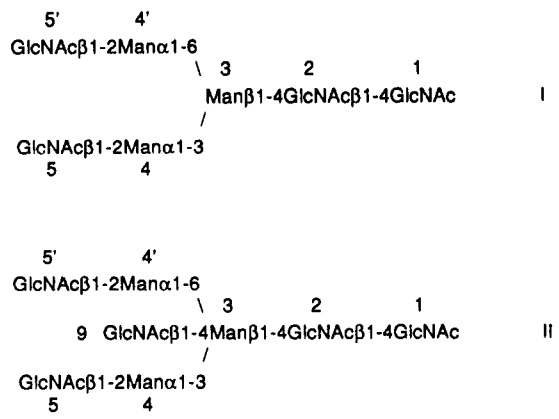

FIGURE 1: Structures of the two oligosaccharides examined in this study.

was previously shown to induce particularly striking conformational transitions about both the Manα1-3Man and Manα1-6Man antennae of the unbisected glycan (Brisson & Carver, 1983c; Homans et al., 1987b), and it is of interest to discover whether such transitions could be detected in the overall dynamic behavior of each glycan.

EXPERIMENTAL PROCEDURES

The glycans GlcNAcβ1-2Manα1-6(GlcNAcβ1-2Manα1-3)Manβ1-4GlcNAcβ1-4GlcNAc (compound **I**, Figure 1) and GlcNAcβ1-2Manα1-6(GlcNAcβ1-2Manα1-3)(GlcNAcβ1-4)Manβ1-4GlcNAcβ1-4GlcNAc (**II**) were isolated from human serotransferrin and hen ovomucoid, respectively, by preparative-scale hydrazinolysis (Patel et al., 1993). The disialylated variant of compound **I** was desialylated by incubation with 50 mM HCl overnight and was then degalactosylated by digestion with 1 unit jack-bean β-galactosidase in 50 mM sodium acetate, pH 5.0, for 5 h at 37 °C. The desired product (**I**) was then purified by passage down a column (1 m × 2.5 cm) of Bio-Gel P4 eluted with water. Compound **II** was separated from the complex mixture of glycans on hen ovomucoid by HPLC using a Dionex model BioLC analyzer equipped with a pulsed amperometric detector.

^{1}H–^{1}H ROESY experiments were performed as described (Homans & Forster, 1992). All molecular mechanical calculations and simulations were performed with the molecular mechanics package DISCOVER (Biosym Technologies Inc.) and were computed *in vacuo* with a dielectric constant ϵ = 80.0 using the force field parametrization described previously (Homans, 1990) but with all torsional terms corresponding to the exo-anomeric potential set to zero (Rutherford et al., 1993). Restrained simulated annealing and restrained molecular dynamics simulations were performed using previously described protocols (Homans & Forster, 1992). Nuclear Overhauser effect distance restraints were classified as strong, medium, or weak and were applied as biharmonic restraints with lower and upper bounds to 1.8–2.7, 1.8–3.3, and 1.8–5.0 Å, respectively. In two cases, constraints involved hydroxymethyl protons which exactly overlapped, and the hydroxymethyl protons were therefore treated as a "pseudoatom" whose coordinates are the mean of those of the two hydroxymethyl protons. Certain investigations described below involved a series of starting configurations for the disaccharide with pseudorandom values of φ and ψ, and these were created by running a dynamics simulation for the disaccharide *in vacuo* at 750 K, followed by rapid quenching to 300 K at 10-ps intervals. In this manner a series of geometries is created which are located in regions of conformational space with relatively low energy, thus avoiding to a large extent problems which arise during minimization of starting structures which are of very high energy.

Table 1: Geometric Parameters for Estimated Global Minimum Energy Configurations of Structures **I** and **II** Derived from Dynamical Simulated Annealing

linkage	φ	ψ	ω
I(a)[a]			
GlcNAcβ1-4GlcNAc	0.6	−33.1	
Manβ1-4GlcNAc	14.9	−27.4	
Manα1-3Man	−34.7	52.3	
GlcNAcβ1-2Manα1-3	13.5	43.6	
Manα1-6Man	−2.0	81.9	179.0
GlcNAcβ1-2Manα1-6	30.2	23.6	
I(b)[b]			
GlcNAcβ1-4GlcNAc	54.3	−1.8	
Manβ1-4GlcNAc	15.0	−5.2	
Manα1-3Man	−62.9	−16.4	
GlcNAcβ1-2Manα1-3	23.5	53.4	
Manα1-6Man	8.1	59.0	−51.6
GlcNAcβ1-2Manα1-6	21.5	18.7	
II			
GlcNAcβ1-4GlcNAc	53.1	−2.3	
Manβ1-4GlCNAc	41.8	−10.3	
Manα1-3Man	−42.4	−18.6	
GlcNAcβ1-2Manα1-3	9.6	26.0	
Manα1-6Man	11.9	−35.9	166.8
GlcNAcβ1-2Manα1-6	26.6	22.5	
GlcNAcβ1-4Man	63.0	5.8	

[a] ω constrained to 180°. [b] ω constrained to −60°.

The torsional angles φ, ψ, and ω are analogous to φ_H, ψ_H, and ω_H in IUPAC convention, and are defined as H1–C1–O1–CX, C1–O1–CX–HX, and H5–C5–C6–O6, where CX and HX are aglyconic atoms.

RESULTS AND DISCUSSION

ROE Measurements in I and II. In order to obtain a series of through-space distance constraints for compounds **I** and **II**, a ^{1}H–^{1}H ROESY spectrum was acquired for each compound at a mixing time τ_m of 300 ms. A total of 13 constraints were obtained for compound **I** and 14 for compound **II**. These were categorized as "weak", "medium", or "strong" (see Experimental Procedures) as indicated in Table 2.

Global Minimum Energy Configuration of I. In order to estimate the global minimum energy configuration of **I**, a series of 10 random geometries was generated for the glycan, and each was used as input to a restrained dynamical simulated annealing protocol, using the ROE constraints listed in Table 2. Two simulations were performed in which an additional angular constraint was included corresponding to ω = 180° or ω = 180° or ω = −60° for residue Man 3. The purpose of these additional constraints was to simulate explicitly the two major rotamer distributions about the C5–C6 bond of Man 3 (Brisson & Carver, 1983c), which we found not to be sampled adequately during molecular dynamics simulations for currently accessible simulation times.

In the case of the simulation with ω = 180°, no single overall conformation was obtained from the simulated annealing protocol. Three of the resulting structures either possessed high energies or had distorted ring geometries, or both, due to the imperfect nature of the simulated annealing strategy. A family of structures could be delineated by superposition of the remaining seven of the 10 initial structures. These comprised similar secondary structures within the core region Manα1-6(Manα1-3)Manβ1-4GlcNAcβ (Figure 2a) and possessed no constraint violations. The reducing terminal GlcNAc and the nonreducing GlcNAc termini were, however, disor-

Table 2: Experimental ROE Constraints for Compounds I and II, Compared with Average ROEs Calculated from the 500-ps Restrained and Free Dynamics Simulations *in Vacuo* of the Same Compounds

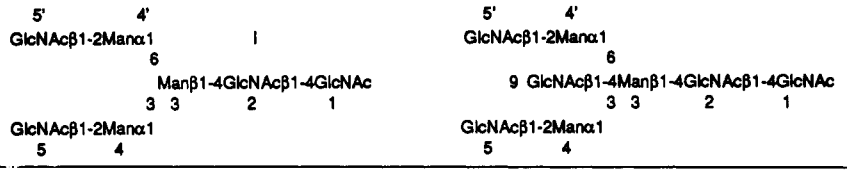

ROE	size[a]	average distance (Å) restr	average distance (Å) free	relative[b] ROE (calc) restr	relative[b] ROE (calc) free	relative ROE (expt)
I(a)[c]						
2-H1–1-H4	S	2.68	3.34	1.22	0.33	n.d.
3-H1–2-H4	S	2.41	2.64	2.31	1.33	n.d.
3-H1–2-H6	W	3.83	4.14	0.14	0.09	0.21
4-H1–3-H3	S	2.48	3.13	1.94	0.48	2.60
4-H1–3-H2	W	3.56	3.45	0.22	0.27	0.14
3-H2–4-H5	M	2.96	4.44	0.67	0.06	n.d.
5-H1–4-H1	S	2.64	3.75	1.33	0.16	1.95
5-H1–4-H2	S	2.74	3.21	1.07	0.41	1.33
4′-H1–3-H6	S	2.54	2.76	2.12	1.02	1.42
4′-H1–3-H6′	W	3.63	4.01	0.25	0.11	0.26
4′-H1–3-H5	W	4.15	4.44	0.11	0.06	0.24
5′-H1–4′–H2	S	2.69	2.83	1.51	0.88	1.42
5′-H1–4′-H1	S	2.82	3.13	1.13	0.48	1.83
I(b)[d]						
2-H1–1-H4	S	2.80	2.91	1.00	0.79	n.d.
3-H1–2-H4	S	2.58	2.46	1.63	2.17	n.d.
3-H1–2-H6	W	3.60	3.59	0.22	0.23	0.21
4-H1–3-H3	S	2.44	2.61	2.28	1.52	2.60
4-H1–3-H2	W	3.69	2.73	0.19	1.16	0.14
3-H2–4-H5	M	2.96	4.44	0.72	0.06	n.d.
5-H1–4-H1	S	2.50	3.34	1.97	0.35	1.95
5-H1–4-H2	S	2.73	3.05	1.16	0.60	1.33
4′-H1–3-H6	S	2.68	2.50	1.78	1.98	1.42
4′-H1–3-H6′	W	3.90	3.69	0.19	0.19	0.26
4′-H1–3-H5	W	2.55	2.50	2.40	1.98	0.24
5′-H1–4′-H2	S	2.74	2.71	1.56	1.22	1.42
5′-H1–4′-H1	S	2.89	3.83	1.13	0.15	1.83
II						
2-H1–1-H4	S	2.58	2.79	1.63	0.98	1.46
3-H1–2-H4	S	2.35	3.54	2.86	0.24	1.66
4-H1–3-H3	S	2.37	2.65	2.72	1.39	2.63
3-H2–4-H5	S	2.69	3.57	1.27	0.23	1.32
5-H1–4-H1	S	2.50	3.28	1.97	0.39	2.02
5-H1–4-H2	S	2.44	3.16	2.28	0.48	2.16
5′-H1–4′-H1	S	2.74	3.45	1.14	0.29	2.13
5′-H1–4′-H2	S	2.57	2.81	1.67	0.98	2.04
9-H1–3-H4	S	2.66	2.67	1.36	1.33	1.44
4-H2–9-H2	M	3.19	3.60	0.46	0.22	0.52
4′-H1–3-H6	S	2.43	2.71	2.34	1.22	1.28
4′-H1–3-H6′	S	3.64	3.49	0.21	0.27	1.28
9-H1–3-H6	S	4.11	4.31	0.10	0.08	1.33
9-H1–3-H6′	S	2.62	2.85	1.49	0.90	1.33

[a] W, weak; M, medium; S, strong. [b] Relative ROEs reported with respect to the intraresidue ROE 4-H1–4-H2, which is taken as 1.00. [c] $\omega = 180°$. [d] $\omega = -60°$.

dered, suggesting additional flexibility in these regions of the molecule. The lowest energy structure of this family was arbitrarily chosen as the consensus starting structure for MD simulations (see below), and relevant conformational parameters for this structure are given in Table 1.

Results similar to the above were obtained in the case of the simulation with $\omega = -60°$, with four "bad" structures, the remainder forming a family with similar secondary structures in the region Manα1-3Manβ1-4GlcNAcβ (Figure 2b), with no constraint violations. In contrast to the above result, two discrete conformations about the Manα1-6Man glycosidic linkage were apparent within this family. As above, the lowest energy structure (Table 1) was chosen as input for MD simulations (see below).

Global Minimum Energy Configuration of II. The global minimum energy conformation of II was estimated in exactly the same manner as that described for I, except that the annealing run with ω restrained to $-60°$ was not performed, commensurate with the known preference for a single conformer at $\omega = 180°$ in the presence of a bisecting GlcNAc residue (Brisson & Carver, 1983c). In this case three bad geometries were generated, and the remaining seven structures formed a family with similar secondary structure for all residues except the reducing terminal GlcNAc residue, which was disordered (Figure 2c). The conformational parameters for the lowest energy consensus structure used as input for MD simulations are given in Table 1.

Average Solution Structure of I. The family of structures derived from the simulated annealing protocol above suggest that I may not exist in solution with a single conformation. In order to assess the regions of conformational space available to the oligosaccharide, each of the two consensus structures

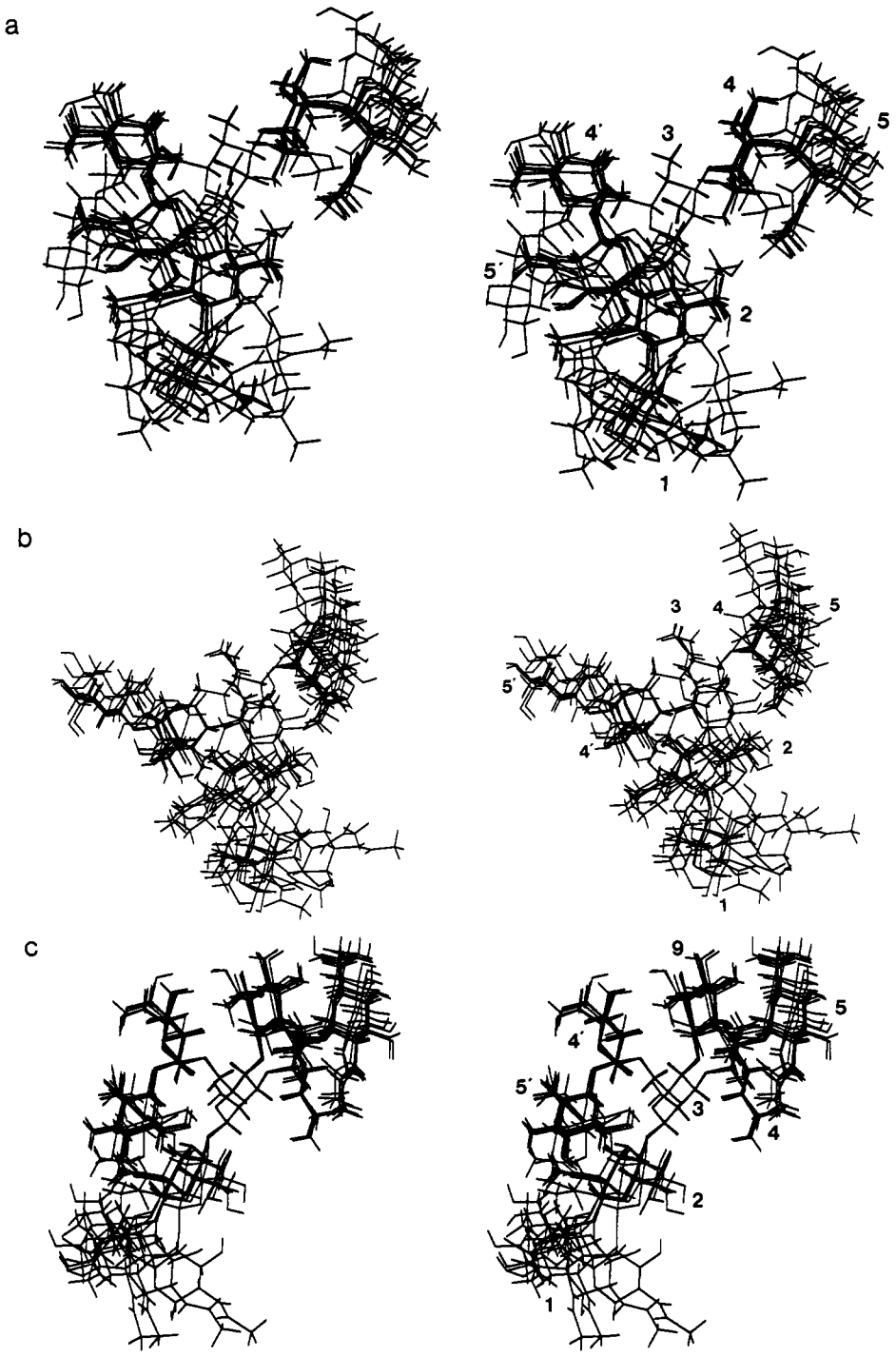

FIGURE 2: (a) Superimposition of the family of seven structures obtained from restrained simulated annealing of 10 random initial starting geometries of compound **I** (see Figure 1), with the dihedral angle ω about the Manα1-6Man linkage constrained to 180°. (b) Superimposition of the family of six structures obtained from restrained simulated annealing of 10 random initial starting geometries of compound **I** (see Figure 1), with the dihedral angle ω about the Manα1-6Man linkage constrained to –60°. (c) Superimposition of the family of seven structures obtained from restrained simulated annealing of 10 random initial starting geometries of compound **II** (see Figure 1), with the dihedral angle ω about the Manα1-6Man linkage constrained to 180°. In each case key residues are identified using the nomenclature given in Table 2.

derived from the simulated annealing protocol was used as input to a 510-ps restrained dynamics simulation *in vacuo*, with identical constraints to those used during simulated annealing, except that the single dihedral constraint about ω was removed. We chose an *in vacuo* simulation, rather than explicit inclusion of solvent water, since the rate of torsional oscillation is known to be much reduced in the latter (Homans, 1990; Rutherford et al., 1993), requiring simulation times larger than are currently accessible in order to sample conformational space adequately. Since our primary objective in the present study was to examine the extent of torsional space mapped by the various oligosaccharides, rather than prediction of conformational fine detail, we consider the approximations inherent in *in vacuo* simulations to be an acceptable compromise.

The instantaneous values of the dihedral angles about each glycosidic linkage over the last 500 ps of each simulation are shown in Figure 3a,c. It is seen that significant torsional oscillations exist about all glycosidic linkages over the time scale of the simulation. In order to determine whether such oscillations might be indicative of the true extent of torsional variation about each glycosidic linkage, ROE values were

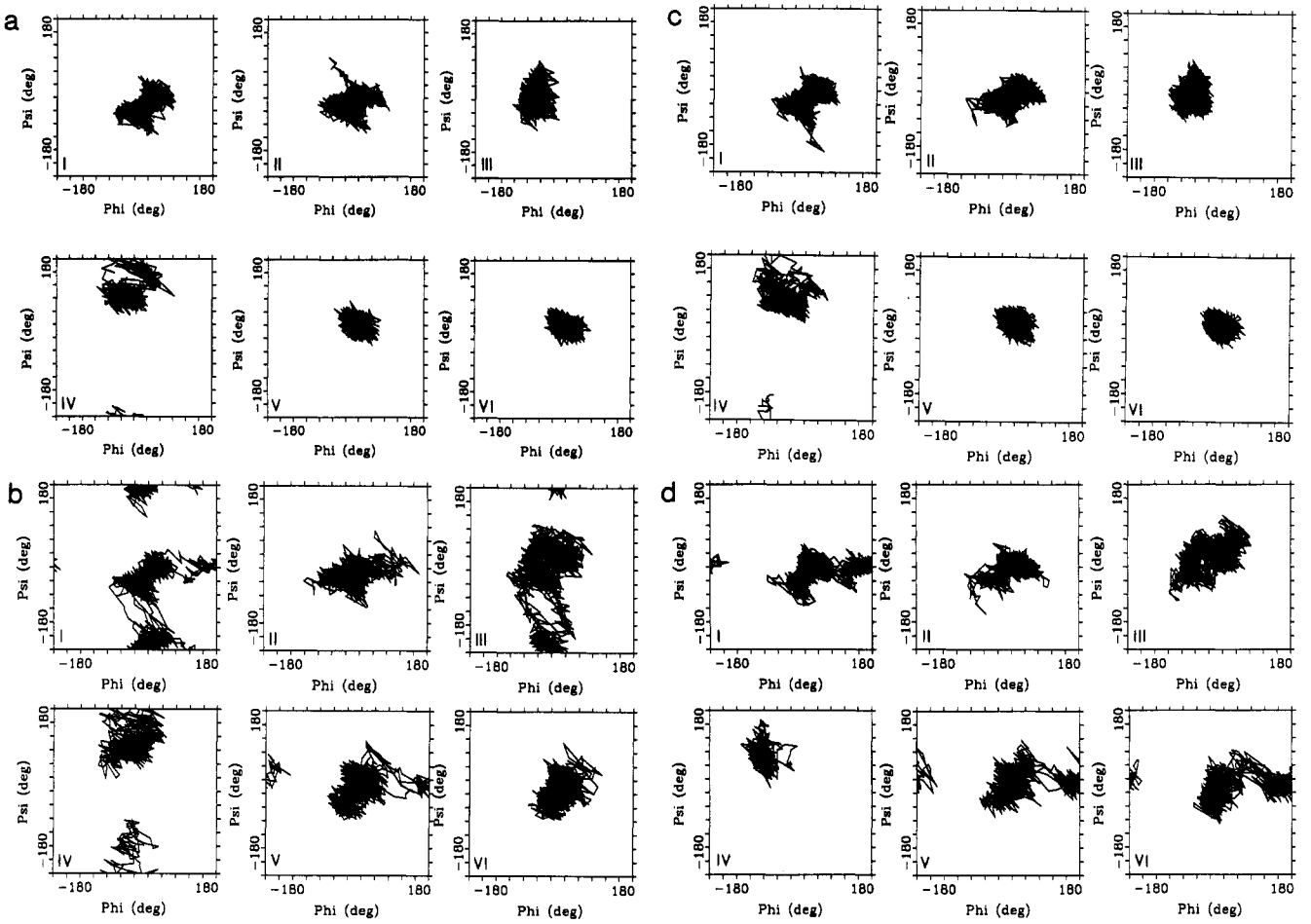

FIGURE 3: φ, ψ plots over the time course of the last 500 ps of the 510 ps *in vacuo* restrained MD simulation of structure I, with starting geometries derived from annealed structures with ω = 180° (a) or ω = –60° (c). Panels refer to the following linkages: (i) GlcNAcβ1-4GlcNAc, (ii) Manβ1-4GlcNAc, (iii) Manα1-3Man, (iv) Manα1-6Man, (v) GlcNAcβ1-2Man (3-arm), (vi) GlcNAcβ1-2Man (6-arm). Shown in b and d are analogous data derived from free dynamics simulations with the same starting geometries.

back-calculated from the simulations using a formalism appropriate for internal motions (Tropp, 1980; Homans & Forster, 1992), which are fast with respect to overall tumbling (Table 2). In all cases where the experimental ROE can be quantified, the computed ROEs agree within a factor of two with the experimental values, which is acceptable in view of the fact that any inherent inaccuracies in the simulation will be magnified to the sixth power by virtue of the distance dependence of the ROE. An exception is the ROE between Man 4′ H-1 and Man 3 H-5, which is underestimated in the first simulation (ω = 180°) and overestimated in the second (ω = 60°). However, since the dihedral angle ω interconverts rapidly between 180° and –60° on the NMR time scale, and since torsional oscillations about the 1–6 glycosidic linkage are coupled to such motions, the predicted value of this ROE is a weighted average of these two values.

The derivation of dynamic data from restrained dynamics simulations is open to criticism. First, it could be argued that the good agreement between ROEs back-calculated from restrained MD simulations and those observed experimentally is unsurprising in view of the fact that the experimental data form part of the theoretical simulation in the form of constraints. However, it is worth noting that even in the presence of the tightest constraint (strong, which allows the distance between two protons to vary between 1.8 and 2.7 Å without energy penalty), the measured relative ROE can vary between ~0.63 and ~7.2, and yet back-calculated ROEs are within the range which is experimentally observed. Of course, multiple constraints can combine with each other, or can combine asymmetrically with minima in energy surfaces, to result in much greater restriction. In this regard it is possible that the presence of restraints masks the true dynamic nature of the molecule, and since the constraint boundaries are applied in an empirical fashion this may be a valid criticism. Unfortunately it is not possible to apply the restraints in a more quantitative manner, since a given ROE can derive from an infinite number of motional models. However, it is at least possible to interpret the data of Figure 3 as representing the minimum extent of torsional oscillations consistent with the experimental data.

In order to estimate the maximum extent of torsional oscillation about each glycosidic linkage, identical simulations were computed, but with all constraints removed (Figure 3b,d). These data do not necessarily represent the maximum extent of torsional oscillation consistent with experimental data, and indeed the computed ROEs in certain cases deviate significantly from the experimental values (Table 2), suggesting that the motional behavior is not indicative of that observed in solution. As described previously, this is a result of the poor performance of the force field parametrization over the full potential surface. We can exclude the possibility that the simulation is of inadequate length, since in every case additional regions of φ, ψ conformational space divorced from the global minimum (and hence statistically visited less often) are being oversampled during the free dynamics simulations. It is the significant population of these regions which gives rise to the deviations of computed ROEs from measured values. Moreover, for the same reason, in certain cases significant ROEs

Table 3: Computed Relative ROEs Predicted from Free Dynamics Simulations of I and II but Which Are Not Observed Experimentally, Together with Predicted Maximum Populations of States

ROE connectivity	relative intensity	state φ, ψ	maximum population (%)[a]
I			
GlcNAc-2 H1–GlcNAc-1 H3[b]	7.40	30, 180	0.9
GlcNAc-2 H1–GlcNAc-1 H5	0.98	30, 180	7.0
GlcNAc-2 H2–GlcNAc-1 H4	0.60	150, 0	11.7
Man 4 H1–Man 3 H4	3.70	0, 180	1.9
Man 4 H2–Man 3 H2	0.52	0, 180	13.5
GlcNAc-5 H2–Man 4 H2	1.00	150, 15	7.0
GlcNAc-5′ H2–Man 4′ H2	1.00	150, 15	7.0
II			
GlcNAc-2 H2–GlcNAc-1 H4	0.60	150, 0	11.7
GlcNAc-5 H2–Man 4 H2	1.00	150, 15	7.0

[a] Calculation based on the limit of detection of the absolute ROE (0.5%), which translates to a relative ROE of 0.07. [b] See Table 2 for nomenclature.

are predicted which are definitely unobservable in solution. For example, in the free dynamics simulation of Figure 3b, the Manα1-3Man linkage spends significant time in the conformation where $\varphi, \psi \sim 0°, 180°$, where signfiicant ROEs would be predicted between Man 4 H-1–Man 3 H-4, and between Man 4 H-2–Man 3 H-2, yet none are observed experimentally. Since the limit of detection of the ROE is known, it is possible to place an upper limit on the populations of these additional conformational states, based on the "unobservable" ROEs alone (Table 3). It is clear from these data that the additional regions of conformational space sampled in free molecular dynamics simulations are severely overestimated in free dynamics simulations. It should be noted that for those conformers where more than one unobservable NOE is identified in Table 3, the smallest predicted population places an upper limit on the population of that conformer. The populations of these conformers are therefore in no case greater than 11.7%, and since these conformers are excluded from restrained dynamics simulations because they give rise to significant constraint violations, these populations are reduced even further when the magnitudes of "observable" ROEs are considered. Thus the restrained molecular dynamics simulations of **I** identify a series of conformations which are consistent with available experimental parameters, and the corresponding average values of φ and ψ are given in Table 4. Of course, these data might represent only one of several alternative dynamic models which are also consistent with experimental data, but since the torsional fluctuations about each glycosidic linkage are within the lowest energy regions of φ, ψ potential surfaces for the analogous disaccharide fragments (Imberty et al., 1991), it is difficult to envisage an alternative motional model that is consistent with experimental data but which is substantially different from that defined here.

The behavior of the free dynamics simulations in unsurprising in view of the fact that no torsional terms have been included in the force field to account for the exo-anomeric effect (Lemieux et al., 1980; Thogersen, 1982; Bock, 1983; Tvaroska & Bleha, 1989). Previously, we parametrized such terms for the current forcefield (Homans, 1990), and while the resulting parametrization gave good results in regions of conformational space close to the global minimum, the torsional space available to glycosidic linkages is severely underestimated when the full potential surface is considered. This behavior derives from the fact the torsional terms were obtained from *ab initio* calculations on dimethoxymethane *in vacuo* (Wiberg & Murcko, 1989). Since the exo-anomeric effect is partially electrostatic in character (Tvaroska & Bleha, 1989), it follows that its magnitude will be attenuated in solution, and hence the relative energy of the exo-anomeric torsional term in the force field should be reduced when considering solution properties. It should be noted that the explicit inclusion of solvent water in the free dynamics simulations would not overcome this difficulty, since the torsional term would still appear at full strength in the energy evaluation scheme. Obviously, it is impossible to determine the extent by which the exo-anomeric term must be reduced, or indeed whether the functional form must be modified, without suitable solution data which are not to hand. In this respect, the inclusion of ROE constraints represents a method whereby the limited solution data which are available can be included, and we suggest that this approach is no less valid than inclusion of an explicit torsional term which could in theory be contrived (e.g., by empirically reducing the torsional barrier of the exo-anomeric term in the current force field) to correct for the inadequacies of free dynamics simulations.

Table 4: Average Values of φ, ψ about Glycosidic Linkages over the Time Course of the 500-ps Restrained MD Simulations *in Vacuo* of (a) GlcNAcβ1-2Manα1-6(GlcNAcβ1-2Manα1-3)Manβ1-4GlcNAcβ1-4GlcNAc and (b) GlcNAcβ1-2Manα1-6(GlcNAcβ1-2Manα1-3)(GlcNAcβ1-4)Manβ1-4GlcNAcβ1-4GlcNAc

linkage	$\langle\varphi\rangle$ (deg)	$\langle\psi\rangle$ (deg)
(a)		
(i)		
GlcNAcβ1-4GlcNAc	27(25)[a]	−17(24)
Manβ1-4GlcNAc	13(26)	−16(20)
Manα1-3Man	−40(15)	12(27)
Manα1-6Man	−8(23)	95(31)
GlcNAcβ1-2Man(α1-6)	26(16)	31(14)
GlcNAcβ1-2Man(α1-3)	25(17)	33(14)
(ii)		
GlcNAcβ1-4GlcNAc	34(27)	−14(22)
Manβ1-4GlcNAc	25(30)	−7(18)
Manα1-3Man	−38(17)	2(23)
Manα1-6Man	−8(27)	79(25)
GlcNAcβ1-2Man(α1-6)	26(15)	36(15)
GlcNAcβ1-2Man(α1-3)	25(15)	28(15)
(b)		
GlcNAcβ1-4GlcNAc	33(14)	6(10)
Manβ1-4GlcNAc	16(24)	−18(18)
Manα1-3Man	−42(12)	−7(13)
Manα1-6Man	0(20)	102.5(39)
GlcNAcβ1-2Man(α1-6)	25(15)	29(14)
GlcNAcβ1-2Man(α1-3)	22(14)	31(14)
GlcNAcβ1-4Man	64(14)	6(10)

[a] Figures in parentheses represent angular rms deviations in degrees for each linkage over the time course of the simulation.

It should be emphasized that the inadequacies demonstrated above are not restircted to the forcefield parametrization utilized here. For example, in a series of gridsearch calculations on a variety of disaccharide fragments using the MM2CARB parametrization, Imberty et al. (1991) described a "relaxed" φ, ψ potential surface for the GlcNAcβ1-2Man fragment which includes a local minimum at φ, ψ = 175°, 20°, at ~1.5 kcal/mol above the global minimum. In this conformation, a large relative ROE of magnitude 6.8 should be observed between GlcNAc H2 and Man H2, and since the population of this conformer based upon the Boltzmann law is ~10%, a relative ROE of magnitude 0.68 is predicted between these protons, yet none is observed in the current study.

Average Solution Structure of II. The average solution structure of **II** was examined in a manner identical to **I** above,

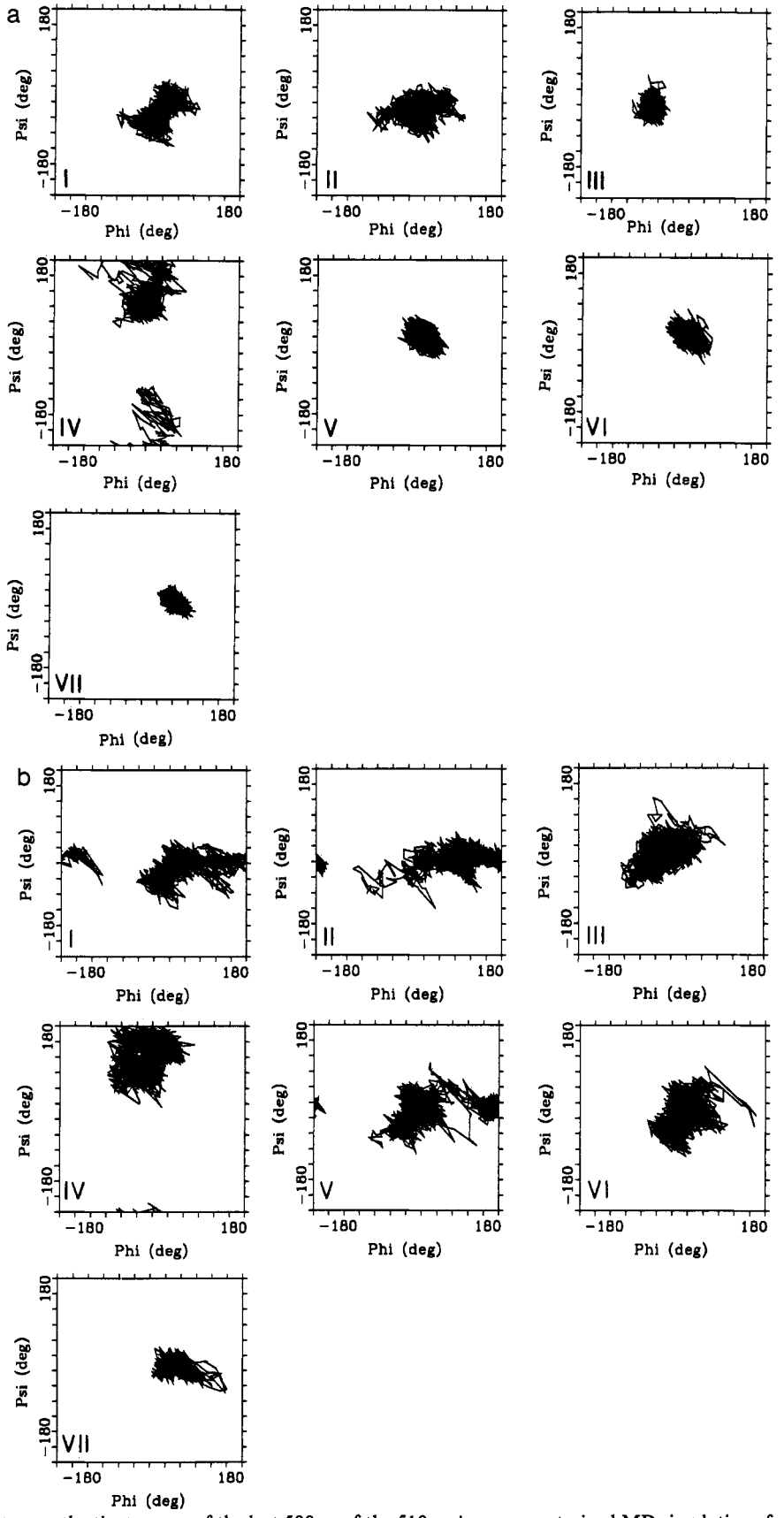

FIGURE 4: (a) φ, ψ plots over the time course of the last 500 ps of the 510 ps *in vacuo* restrained MD simulation of structure **II**, with starting geometry derived from annealed structure with $\omega = 180°$. Panels refer to the following linkages: (i) GlcNAcβ1-4GlcNAc, (ii) Manβ1-4GlcNAc, (iii) Manα1-3Man, (iv) Manα1-6Man, (v) GlcNAcβ1-2Man (3-arm), (vi) GlcNAcβ1-2Man (6-arm), (vii) GlcNAcβ1-4Man. Shown in b are analogous data derived from a free dynamics simulation with the same starting geometry.

and the instantaneous values of φ, ψ for each linkage over the time course of the final 500 ps of the restrained and free MD simulations are shown in Figure 4. In common with **I**, additional regions of conformational space are explored by certain linkages in the free dynamics simulation of **II** (Figure 4b), and the average ROEs derived from the free dynamics

simulation are generally in poorer agreement with those derived experimentally (Table 2). The maximum predicted populations of the additional states observed in free dynamics simulations are included in Table 3. Since these populations are again small, experimentally "reasonable" conformations of II would appear to be identified by the restrained dynamics simulations, and the corresponding average values of φ and ψ are given in Table 4. An exception is the extent of torsional variation about the Man4′–Man 3 glycosidic linkage, for which the back-calculated ROE from Man4′-H1–3-H6/3-H6′ is in relatively poor agreement with experiment. This is an inevitable consequence of the fact that the H6 protons of Man 3 exactly overlap in structure II. It is therefore necessary to treat these protons as a pseudoatom (see methods) when applying experimental constraints, which can result in a significant error.

Comparison of Average Solution Structures of I and II. It is seen from Figures 3 and 4 that the dynamic behavior of I and II in solution is predicted to be similar for most glycosidic linkages. Apart from the well-known differences between the rotamer distributions about the C5–C6 bond of Man 3 in both compounds which was not explicitly examined in this study, the only glycosidic linkages which have substantially different solution dynamics between the structures are Manα1-6Man and Manα1-3Man. Each linkage appears to be considerably constrained by the presence of the bisecting GlcNAc residue. The Manα1-6Man linkage is restrained by virtue of the restriction of ω to 180°, whereas the bisecting GlcNAc appears to exert a direct steric influence in the case of the Manα1-3Man linkage. The dynamic variation of the Manα1-3Man linkage is particularly apparent from the observed experimental data. For example, the small ROE (0.14) which is observed between Man 4 H-1 and Man 3 H-2 in I is not observed in II, consistent with the larger effective distance in II. It should be noted that the ROE observed in I can definitely be assigned as a direct effect (rather than a three-spin effect) from the sign of the ROE, in complete analogy to that observed in the galactosylated analogue of I (Homans et al., 1987b). The simulations predict that the ROE between Man 3 H-2 and Man 4 H-5 should be larger in II, commensurate with the smaller effective distance between these protons. However, since in I, Man 4 H-5 overlaps with Man 3 H-3, which also experiences an ROE from Man 3 H-2, it is impossible to quantify the ROE between Man 3 H-2 and Man 4 H-5 with sufficient accuracy for meaningful comparison.

In addition to differences in ROE intensities across the Manα1-3Man linkage between I and II, characteristic chemical shift differences are also apparent in the vicinity of this linkage. In a previous study of related N-linked glycans, these differences were attributed to different "rigid" conformations about the Manα1-3Man linkage in I and II (Homans et al., 1987b). Since the average conformations defined in the present study are similar to previously defined rigid conformations, i.e., $\varphi, \psi \sim -20°, +30°$ in I and $-40°, -15°$ in II, it is possible to explain these shift differences in the same fashion but in terms of the different average conformations. Thus, in I, the average location of the ring oxygen of Man 4 is proximal to Man 3 H-2, resulting in deshilding and downfield shift, whereas this oxygen is further from Man 3 H-2, and closer to Man 3 H-3 in II, resulting in an upfield shift of Man 3 H-2 and a downfield shift of Man 3 H-3.

CONCLUSIONS

As in our previous study on a model disaccharide (Rutherford et al., 1993), we found that the application of free dynamics simulations in the determination of the dynamic behavior of GlcNAcβ1-2Manα1-6(GlcNAcβ1-2Manα1-3)-Manβ1-4GlcNAcβ1-4GlcNAc and GlcNAcβ1-2Manα1-6(GlcNAcβ1-2Manα1-3)(GlcNAcβ1-4)Manβ1-4GlcNAcβ1-4GlcNAc gives rise to a motional model which does not accord with available experimental data. Conversely, the results of restrained dynamics simulations yield models which are consistent with available experimental data and importantly predict to a good approximation measurable experimental parameters which are not originally included as restraints. While it is therefore tempting to suggest that such restrained simulations provide a good approximation to the true solution dynamics, we emphasize that in view of the empirical nature of the applied NOE constraints, this approach is not ideal, and strictly the only conclusion that can be drawn is that the resulting dynamic model represents the minimum extent of internal motion which is consistent with experimental data. Nevertheless, a molecular mechanical force field parametrization of sufficient accuracy to define oligosaccharide dynamics has not been forthcoming, and on the basis of the present study we suggest that the restrained dynamics method is a useful approach for approximating solution behavior of oligosaccharides.

It is of interest that the average structures of I and II derived in the present study are in good agreement with the rigid geometeries previously determined from ROE and spin-coupling constant data together with semiempirical molecular orbital calculations (Homans et al., 1986, 1987b). In particular, the two conformations about the Manα1-3Man linkage observed in previous work resulting from the presence or absence of the bisecting GlcNAc residue correspond with similar average conformations about the Manα1-3Man linkage. In retrospect, therefore, it would appear that the rigid geometry approximation, at least for I and II, resulted in structures which were a good approximation to the average solution conformations of these molecules.

REFERENCES

Bock, K. (1983) *Pure Appl. Chem. 55*, 605.

Bock, K., Arnarp, J., & Lonngren, J. (1982) *Eur. J. Biochem. 129*, 171.

Brisson, J.-R., & Carver, J. P. (1983a) *Biochemistry 22*, 1362.

Brisson, J.-R., & Carver, J. P. (1983b) *Biochemistry 22*, 3671.

Brisson, J.-R., & Carver, J. P. (1983c) *Biochemistry 22*, 3680.

Bush, C. A. (1992), *Curr. Op. Str. Biol. 2*, 655.

Bush, C. A., & Cagas, P. (1992) *Adv. Phys. Chem. 2*, 149.

Cagas, P., & Bush, C. A. (1992) *Biopolymers 32*, 277.

Cumming, D. A., & Carver, J. P. (1987a) *Biochemistry 26*, 6664.

Cumming, D. A., & Carver, J. P. (1987b) *Biochemistry 26*, 6676.

Homans, S. W. (1990) *Biochemistry 29*, 9110.

Homans, S. W., & Forster, M. (1992) *Glycobiology 2*, 143.

Homans, S. W., Dwek, R. A., Fernandes, D. L., & Rademacher, T. W. (1982) *FEBS Lett. 150*, 503–506.

Homans, S. W., Dwek, R. A., Fernandes, D. L., & Rademacher, T. W. (1983) *FEBS Lett. 164*, 231–235.

Homans, S. W., Dwek, R. A., Boyd, J., Mahmoudian, M., Richards, W. G., & Rademacher, T. W. (1986) *Biochemistry 25*, 6342.

Homans, S. W., Dwek, R. A., & Rademacher, T. W. (1987a). *Biochemistry 26*, 6571–6578.

Homans, S. W., Dwek, R. A., & Rademacher, T. W. (1987b) *Biochemistry 26*, 6553.

Imberty, A., Tran, V., & Perez, S. (1989) *J. Comput. Chem. 11*, 205.

Imberty, A., Delage, M.-M., Bourne, Y., Cambillau, C., & Perez, S. (1991) *Glycoconj. J. 8*, 456.

Imberty, A., Perez, S., Hricovini, M., Shah, R. N., & Carver, J. P. (1993) *Int. J. Biol. Macromol. 15*, 17.
Lemieux, R. U., Delbaere, L. T. J., Koto, S., & Rao, V. S. (1980) *Can. J. Chem. 58*, 631.
Miller, K. E., Mukhopadhyay, C., Cagas, P., & Bush, C. A. (1992) *Biochemistry 31*, 6703.
Patel, T., Bruce, J., Merry, A., Bigge, C., Wormald, M., Jaques, A., & Parekh, R. (1993) *Biochemistry 32*, 679–693.
Paulsen, H., Peters, T., Sinnwell, V., Heume, M., & Meyer, B. (1986) *Carbohydr. Res. 156*, 87.
Poppe, L., & van Halbeek, H. (1992) *J. Am. Chem. Soc. 114*, 1092.
Rutherford, T. J., Partridge, J., Weller, C., & Homans, S. W. (1993) *Biochemistry 32*, 12715–12724.
Sabesan, S., Bock, K., & Lemieux, R. U. (1984) *Can. J. Chem. 62*, 1034.
Thogersen, H., Lemieux, R. U., Bock, K., & Meyer, B. (1982) *Can. J. Chem. 60*, 44.
Tropp, J. (1980) *J. Chem. Phys. 72*, 6035.
Tvaroska, I., & Bleha, T. (1989) *Adv. Carbohydr. Chem. Biochem. 47*, 45.
Wiberg, K. B., & Murcko, M. A. (1989) *J. Am. Chem. Soc. 111*, 4821.
Yan, Z.-Y., & Bush, C. A. (1990) *Biopolymers 29*, 799.